



Use of *Tilia* extract to improve the optical and electrochemical properties of ZnO semiconductor nanoparticles

H. E. Garrafa-Gálvez¹, L. Cardoza-Avenidaño^{1,*}, R. M. López-Gutiérrez¹, M. E. Martínez-Rosas¹, F. N. Murrieta-Rico², and P. A. Luque^{1,*} 

¹Facultad de Ingeniería, Arquitectura y Diseño, Universidad Autónoma de Baja California, 22860 Ensenada, BC, Mexico

²Universidad Politécnica de Baja California, Ingeniería Mecatrónica, 21376 Mexicali, Baja California, Mexico

Received: 21 June 2022

Accepted: 30 October 2022

© The Author(s), under exclusive licence to Springer Science+Business Media, LLC, part of Springer Nature 2023

ABSTRACT

In order to meet the growing demand for new technologies, new materials with improved electrical, electronic, and electrochemical properties are needed. In the present work, the biosynthesis of zinc oxide nanoparticles was carried out with the aid of *Tilia* extract, varying the amount of extract used to obtain unique properties. The amounts of extract used were 1, 2, and 4% (volume ratio of water/weight of *Tilia*). The nanoparticles were characterized by FTIR, TEM, XRD, UV–Vis, and EIS. The analyses revealed that the nanoparticle composition includes organic material components from the *Tilia* extract. The average sizes shown by the nanoparticles were 41.8, 38.5, and 33.2 nm. XRD analyses determined that the nanoparticles have a hexagonal structure with a Wurtzite phase and crystallite sizes of 30.97 nm for 1%, 28.62 nm for 2%, and 14.52 nm for 4%. For the optical properties, the band gap values of the samples were 2.80, 2.64, and 2.47 eV for 1, 2, and 4%, respectively. Due to these characteristics, the obtained nanoparticles presented outstanding electrochemical properties that could benefit optoelectronic devices.

1 Introduction

Zinc oxide (ZnO) is one of the most important semiconducting materials, having a wide band gap (3.30 eV) and good exciton-binding energy (60 meV) [1]. It is used in numerous applications such as sunblocks, paints, cosmetics, and optoelectronic devices [2]. There exists a great number of methods for obtaining ZnO nanoparticles [3]. The main issue

regarding the current ones is the costly and toxic reactants used [4], making necessary the use of more environmentally friendly and cheaper methods that also improve the properties of the synthesized nanoparticles. One of the most important methods to attain these goals is biosynthesis [5]. Biosynthesis is a method in which toxic reactants are avoided by substituting them for fungi, bacteria, and plants [6]. For the biosynthesis of ZnO nanoparticles, several

Address correspondence to E-mail: lcardoza@uabc.edu.mx; pluque@uabc.edu.mx

natural stabilizing agents have been reported as the ones published by Velsankar et al. in 2019, who utilized *Curcubita* seed extracts [7]. In 2020 Sheik Mydeen et al., reported the preparation of ZnO nanoparticles with the aid of *Prosopis juliflora*, helping their antibacterial and photocatalytic properties [8]. In 2021 the use of *Sonneratia alba* was reported by Mujahid, which increased the antioxidant activity and anti-inflammatory properties of the nanoparticles obtained [9]. *Tilia* extract has previously been used in the biosynthesis of nanoparticles such as Cu [10], AgCl [11], Ag [12], CuO [13], and Au [14] nanoparticles, among others. However, to this date, there is no account of the use of *Tilia* for the biosynthesis of ZnO nanoparticles. *Tilia* is a plant native to Europe and Western Asia. Among its main active ingredients are flavonoids, mucilage, volatile oil, phenolic acids, amino acids, and others. *Tilia* flowers are used to treat muscle spasms, as expectorant, and to heal cold flus [15]. In this investigation, green synthesis of ZnO nanoparticles was carried out using different amounts of *Tilia* extract, which works as stabilizing agent. The as-obtained nanoparticles were characterized through different techniques to reveal their composition, structure, morphology, and optical properties and were characterized through electrochemical impedance spectroscopy (EIS) to know the electrochemical properties they present.

2 Experimental

2.1 Materials

Dry *Tilia* and deionized water were used to obtain the *Tilia* extract. For the biosynthesis of the nanoparticles, *Tilia* extract, zinc nitrate hexahydrate ($\text{Zn}(\text{NO}_3)_2 \cdot 6\text{H}_2\text{O}$) 99% (Sigma Aldrich), and deionized water were used.

2.2 Extract preparation

For extract preparation, different quantities of dry *Tilia* were weighed (0.5, 1, and 2 g). Afterward, 50 mL of deionized water were added and stirred at room temperature for 2 h; the solutions were labeled 1, 2, and 4%, respectively. After that time, the solutions were placed in a hot water bath at 60 °C for 1 h. Filtration with Whatman #4 paper was followed to

remove the remaining *Tilia* solids and to obtain the final extract solutions.

2.3 Synthesis

For the biosynthesis of the nanoparticles, 2 g of $\text{Zn}(\text{NO}_3)_2 \cdot 6\text{H}_2\text{O}$ were added to the previously prepared solutions (1, 2, and 4%) and stirred for 1 h. Subsequently, the different solutions were set in a 60 °C hot bath for 13 h until all the liquid was evaporated. The as-obtained material was given a thermal treatment at 400 °C for 1 h. Finally, the ZnO nanoparticles were obtained and labeled TL1, TL2, and TL4 according to the percentage of extract used (1, 2, and 4%, respectively). The described procedure is depicted graphically in Fig. 1.

2.4 Materials and methods

Powder corresponding to each of the three samples (labeled 1%, 2%, and 4%) was compressed under a pressure of 312 GPa for 30 min, and three pellets were obtained. Each had a 1 mm width ($l = 1$ mm) and a 10 mm diameter ($d = 10$ mm). The pellets were placed, respectively, between two polished copper electrodes in order to model a parallel plate capacitor. The samples were connected to an E4980A Precision LCR Meter. As a result, a set of data corresponding to magnitude of total impedance $|Z_T|$, phase angle θ_d , and frequency values were obtained. The measurements were obtained at room temperature, which can be considered 25 °C.

2.5 Characterization

The obtained nanoparticles were characterized through a Perkin Elmer-Fourier transform infrared (FTIR) spectrometer with a 0.5 cm^{-1} resolution within a 400 to 3500 cm^{-1} measurement range. A JEOL JEM-2010F transmission electron microscope (TEM) was used at an accelerating voltage of 120 kV. A Bruker D2-Phase Kit X-ray diffractometer (XRD) was run at 30 kV, 10 mA, 1 s/step, and $2^\circ/\text{min}$. A Perkin Elmer Lambda 365 UV-Vis spectrometer was operated within the 800–190 nm range and with a scanning speed of 600 nm/min. And, a LCR Precision E4980A electrochemical impedance spectroscopy (EIS) was used.

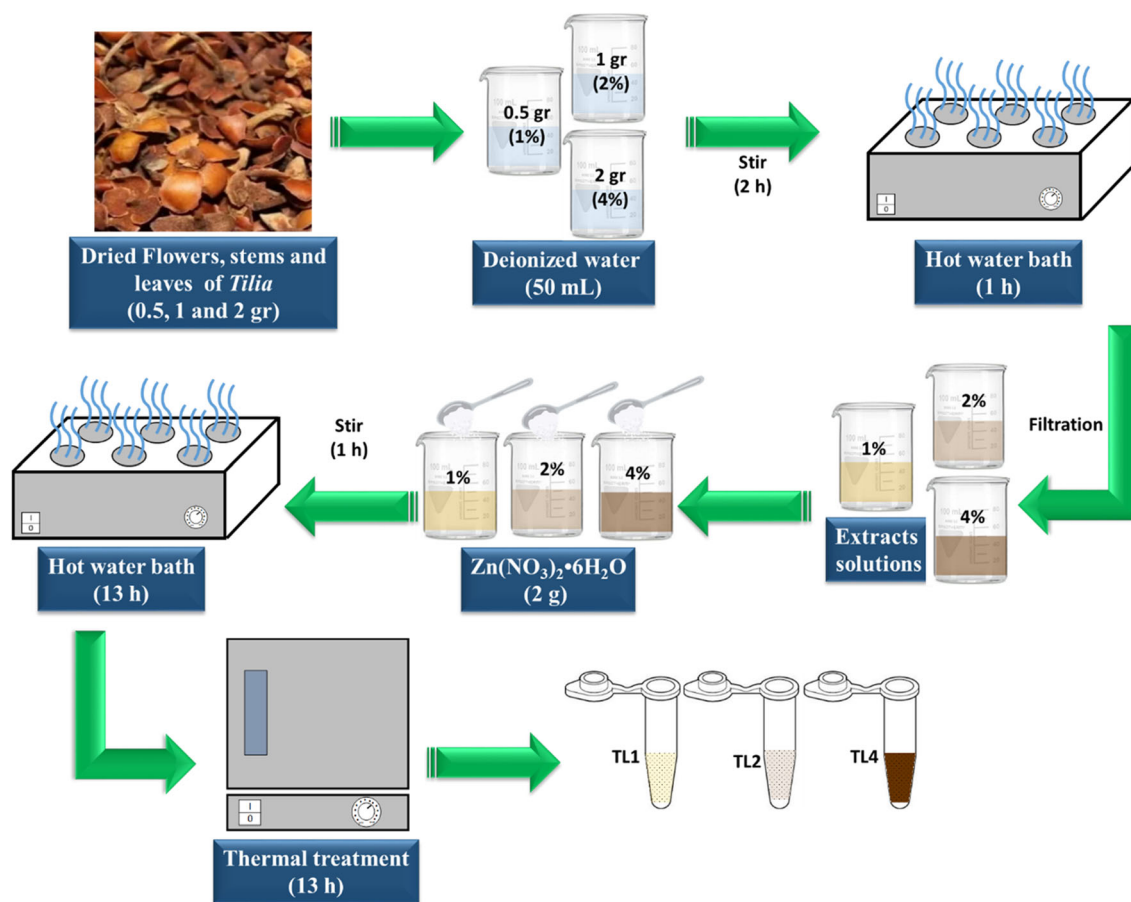


Fig. 1 Graphical representation of ZnO nanoparticles preparation process using *Tilia* extract

3 Results

3.1 FTIR

The FTIR analyses were carried out, and the results are shown in Fig. 2. It can be seen that for TL1, TL2, and TL4, there is a very intense band at 400 cm^{-1} . This band is assigned to the stretching vibration mode of the Zn–O bond [16]. The presence of this band indicates the formation of ZnO nanoparticles for the three samples. Within the 770 a 1640 cm^{-1} range, a set of bands is shown due to the different vibrations of the C–C, C=C, C–O, C=O [17]. These bands belong to different organic components of the *Tilia* extract, within which phenolic acids, flavonoids, polyphenols, etc. are found [18]. These bands indicate that when nanoparticle formation occurs, some *Tilia* extract components remain as well. Furthermore, it can be noted that as the amount of extract increases from 1 to 4%, the assigned bands of extract organic molecules are enhanced in intensity and are further

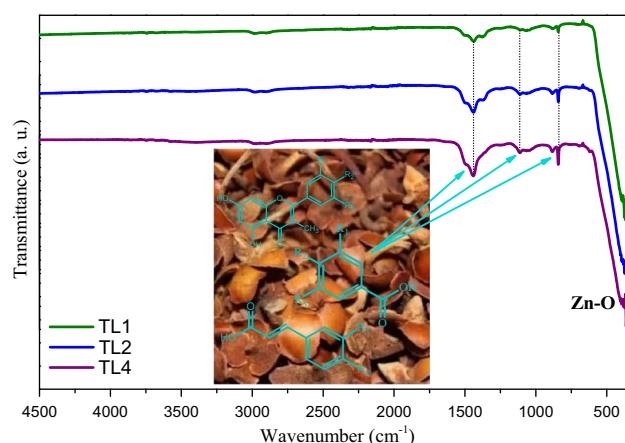


Fig. 2 FTIR analysis of the TL1, TL2, and TL4 ZnO nanoparticles

defined. The findings confirm that using a greater amount of extract translates into a greater amount of organic molecules in the final product.

3.2 Morphological properties

The shape of the TL1, TL2, and TL4 nanoparticles was studied, and the results are shown in Fig. 3. For all samples, similar shapes were displayed, depicting nanoparticles of quasi-spherical shape (Fig. 3a, d, g) with size distribution that varied from 20 to 69 nm. The average calculated diameters were 41.8, 38.5, and 33.2 nm for TL1, TL2, and TL4, respectively (Fig. 3c, f, i). As the concentration of *Tilia* extract used in the biosynthesis increased, the diameter decreased. This effect is due to organic molecules from the extract functioning as stabilizing agents that prevent the nanoparticles from agglomerating and growing in size [19], as reported in various ZnO biosynthesis studies [30]. The formation of ZnO nanoparticles that was revealed through FTIR was supported by HRTEM (Fig. 3b, e, h) since TL1, TL2, and TL4 presented a lattice fringe of 0.25 nm, which is attributed to the (002) plane from the Wurtzite phase of the ZnO nanoparticles crystallized through this synthesis process [20, 21].

3.3 XRD

The crystalline structure analysis of the samples was carried out, and the results are disclosed in Fig. 4. In the samples diffraction patterns, it was found that TL1, TL2, and TL4 displayed peaks at 31.8, 34.5, 36.3, 47.6, 56.6, 62.9, and 68.1 $^{\circ}$. These peaks can be indexed to the (100), (002), (101), (102), (110), (103), and (112) planes, respectively [22]. The set of peaks belongs to ZnO with a hexagonal structure of a Wurtzite phase [23] according to the JCPDS #79-2205 crystallographic card [24, 25]. These results are in good correlation with the HRTEM results. Crystallite sizes of TL1, TL2, and TL4 were estimated through the Scherrer model (Eq. 1) [26],

$$D = \frac{K\lambda}{\beta \cos(\theta)} \quad (1)$$

where D is the average crystallite size, K is the shape factor considered as 0.9, λ is the wavelength of the incident x-ray, β is the full width at half maximum height of the peak, and θ is the diffraction angle of the rays. The crystallite size estimations of TL1, TL2, and TL4 were 30.97, 28.62, and 14.52 nm, respectively, similar to those reported in the literature for this type of nanoparticles [27, 28]. Moreover, it is possible to

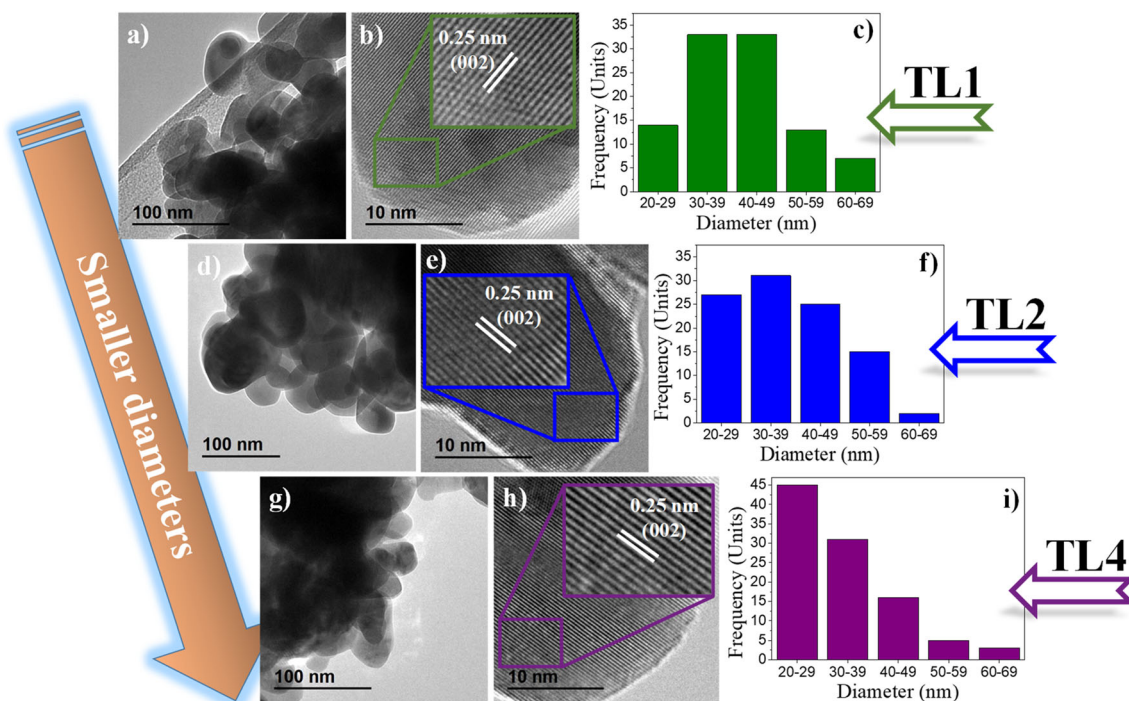


Fig. 3 TEM (a, d, and g) and HRTEM (b, e, and h) micrographs and diameter size distribution of the TL1, TL2, and TL4 ZnO nanoparticles (c, f, and i)

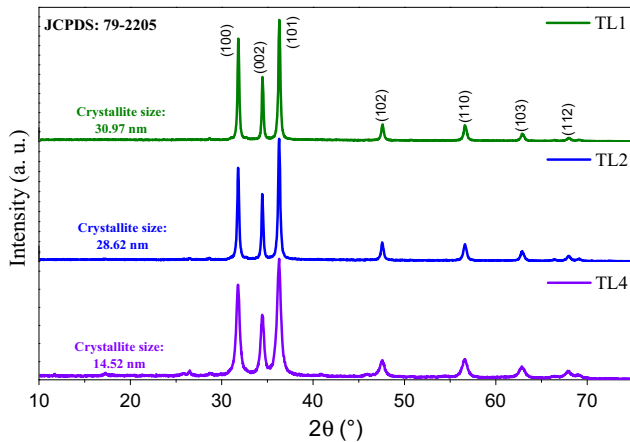


Fig. 4 Diffractograms obtained by XRD of the TL1, TL2, and TL4 ZnO nanoparticles

note that as the amount of extract used increased, the crystallite size diminished, following the same tendency disclosed through the TEM analysis. It was proven that by changing the amount of extract utilized, it was possible to manipulate the diameter size of the nanoparticles and the crystallite size of the final products. Rietveld refinement was performed to calculate some of the characteristics of TL1, TL2, and TL4. The results are shown in Table 1. The crystalline structure and space group remained the same throughout the samples. TL4 rendered the highest value for lattice strain. The increase in lattice strain is attributed to the interaction between nanoparticles and organic molecules from the *Tilia* extracts.

3.4 Optical properties

The analysis of the optical properties was performed by the UV–Vis spectrophotometry technique; the results are illustrated in Fig. 5. The UV–Vis absorbance spectrograms (Fig. 5a) for TL1, TL2, and TL4 depicted a band at 374 nm. This band is attributed to the characteristic surface plasmon resonance [29, 30] of Wurtzite phase ZnO nanoparticles, as established in the literature [31, 32]. Therefore, it indicated

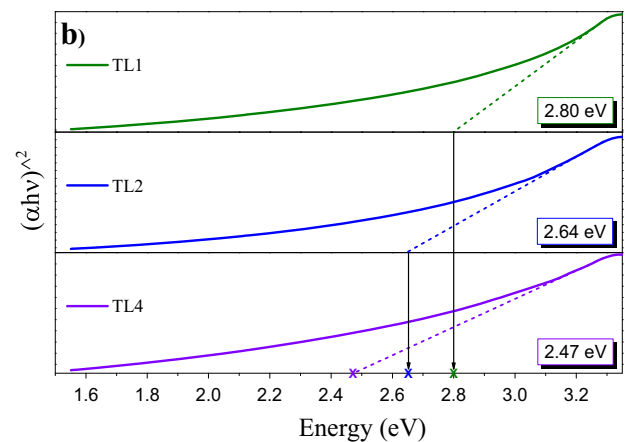
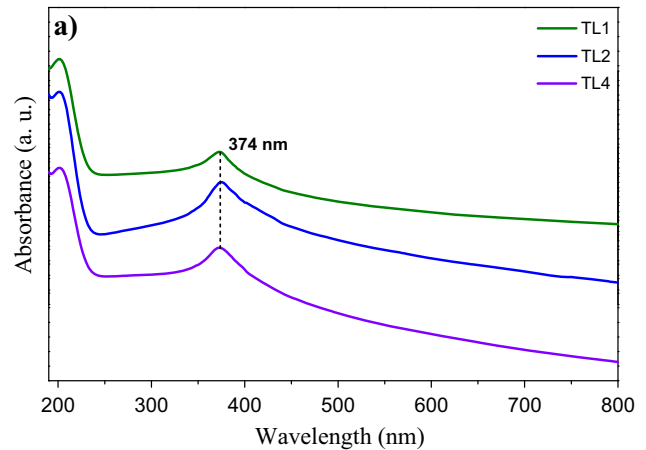


Fig. 5 Assessment of the optical properties through **a** UV–Vis spectroscopy and **b** Tauc model of the TL1, TL2, and TL4 ZnO nanoparticles

the formation of ZnO nanoparticles for TL1, TL2, and TL4. The materials optical properties were supplemented by estimating their band gap values. The band gap is defined as the energy required to promote an electron from the valence band to the conduction band. The Tauc model, Eq. 2, was implemented for this calculation:

$$(\alpha h\nu)^{\frac{1}{n}} = A(h\nu - E_g), \tag{2}$$

where h is Planck’s constant, ν is the photon frequency, α is the absorbance coefficient that relates to

Table 1 Results obtained by Rietveld refinement

Sample	Crystalline structure	Space group	ϵ (%)	Density (g/cm ³) (calculated)
TL1	Hexagonal	P 63 m c	0.338	5.6120
TL2	Hexagonal	P 63 m c	0.311	5.6587
TL4	Hexagonal	P 63 m c	0.604	5.6413

the sample’s nature and the trajectory of the photon beam, E_g is the band gap, A is a dimensionless constant, and n denotes the nature of the electronic transition (1/2 for direct allowed transitions, 3/2 for direct forbidden transitions, 2 for indirect allowed transitions, and 3 for indirect forbidden transitions) [33]. The ZnO nanoparticles have a direct allowed type of transition; hence the value for n was considered 1/2.

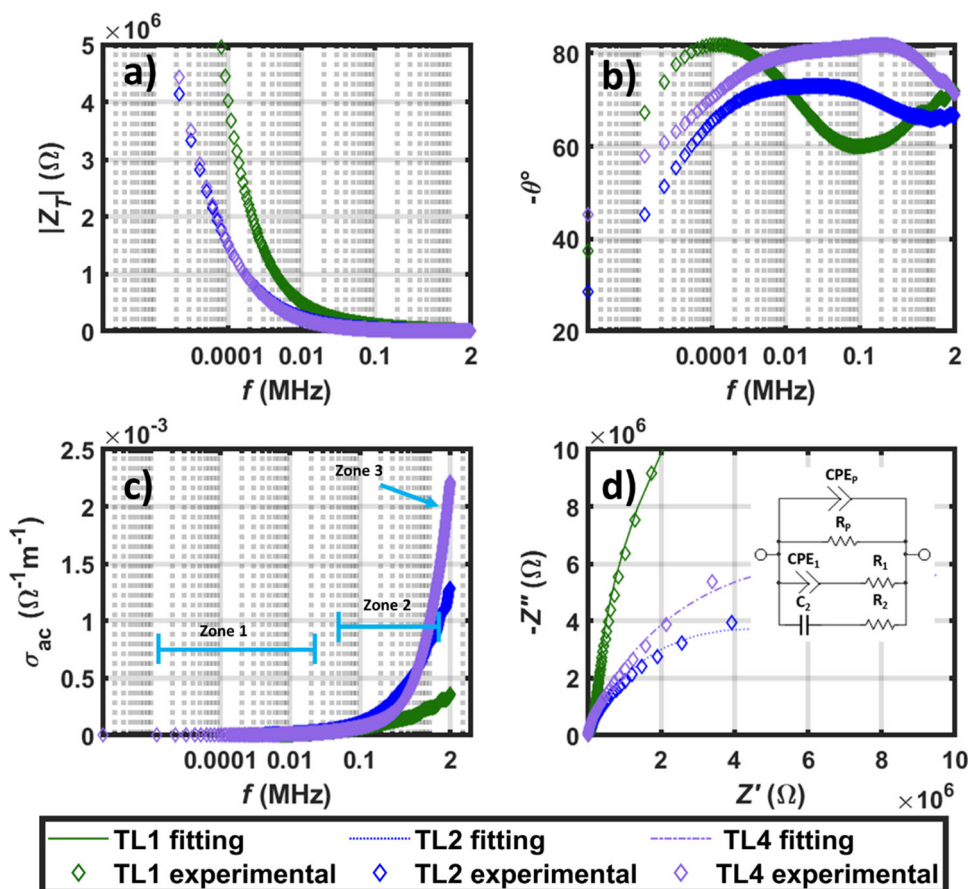
The results conveyed by the Tauc model can be observed in Fig. 5b. It is disclosed that by adding any amount of *Tilia* extract, the band gap is consequently modified in comparison to commercial ZnO (approximately 3.30 eV) [34]. The values were found to be 2.80, 2.64, and 2.47 eV for TL1, TL2, and TL4, respectively. It is proven that by varying the amount of *Tilia* extract used, it is possible to manipulate the structural and electronic properties of the ZnO nanoparticles. This has been manifest in different reported investigations where biosynthesis has been executed to attain ZnO nanoparticles [35]. The results achieved through the various characterization techniques of the obtained nanoparticles gave way to

analyzing TL1, TL2, and TL4 by electrochemical impedance spectroscopy to further detail their electrochemical properties.

3.5 Electrochemical testing

From the direct measurement of impedance magnitude, experimental data for each sample are retrieved. The impedance data of samples TL2 and TL4 show similar behavior, but the data corresponding to TL1 is significantly different from the other two samples (Fig. 6a); this, for samples TL2 and TL4, is an indicative of a similar relationship—of the real and imaginary parts. In the case of TL1, the impedance spectra difference indicates different conductive processes inside the sample TL1 compared to TL2 and TL4. When observing the phase angle from the direct measurements, the similarity in the frequency response for samples TL2 and TL4 is confirmed, where the local minimum phase angle is observed, for each case, to be in the frequency range corresponding to 8.42 and 629 kHz.

Fig. 6 Electrochemical impedance spectroscopy results of analyzed sample: Bode plots of impedance (a), phase (b), total conductivity (c), and Nyquist plot (d) of real and imaginary impedance values



For TL1, the local minimum phase angle is observed to lie within the 320 Hz and 4.12 kHz range. For samples TL2 y TL4, there is a similar behavior in how the reactive and resistive effects act, but there is a difference in the magnitude of these effects; this is expressed in the phase angle as local minimums at almost the same frequency values. Furthermore, a local maximum is observed for TL1 near the local minimums of TL2 and TL4. This is a consequence of a different relation between the magnitude of reactive effects in sample TL1 compared to TL2 and TL4.

The AC conductivity of each sample is shown in Fig. 6c. The relationship between the AC conductivity σ_{ac} and the DC conductivity σ_{dc} is given by Jonsher's power law [36]:

$$\sigma_{ac} = \sigma_{dc} + A\omega^n, \quad (3)$$

where A is the pre-exponential factor, ω is the angular frequency, and n is the frequency exponent, which defines how the transition from σ_{dc} to σ_{ac} is. After using the conductivity data, the Eq. 3 was implemented as "user-defined" for non-linear fitting in OriginPro 2019. Then, Eq. 3 was fitted to data shown in Fig. 6c, and as a result, the parameters of Jonsher's power law were estimated for each sample, where all the data points of f, σ_{ac} were considered. The results are presented in Table 2.

For all samples, the AC conductivity increased when the frequency was increased (Fig. 6c). However, three zones can be differentiated in the conductivity behavior of each sample. The first zone corresponds to the DC conductivity, an almost constant value. In this regard, σ_{dc} denotes where the fitted equation intersects the ordinate axis. The DC conductivity represents a zone in the observed conductivity where there is no slope, in particular, σ_{dc} is in the 20 to 100 kHz range. For these samples, the DC conductivity is expected to be almost the same from the data in the impedance spectra and the phase plot. However, although the samples TL2 and TL4 have close values of σ_{dc} , TL1 has a value an order of magnitude below TL2 and TL4, which is confirmed in the numerical value presented in Table 2. For the

same two samples, zone 2 is the transition from constant value (DC conductivity) to the asymptotic behavior, which is observed for the AC conductivity of TL2 and TL4.; in these two cases, the transition differs in the growth rate, this is observed in the exponent magnitude (n). Conductivity of both these samples follow the universal behavior associated to Jonsher's power law. In addition, for these two samples, the n lies between 0.6 and 1, characteristic of ionic compounds [37]. In the case of TL1, only two zones are observed, the DC conductivity and the transition zone, the asymptotic behavior is not observed, and it could be expected to appear at frequencies higher than 2 MHz. Nevertheless, the same behavior is observed for the AC conductivity of all samples, which coincides with what was expected for ionic compounds.

As it has been reported elsewhere [36–39] for ZnO NPs with the above-mentioned morphology, the observed electrical behavior can be modeled through the electrical circuit shown in the inset of Fig. 6d. Electrical characterization and modeling results are defined by the sample properties, such as particle size or semiconductor properties. As it is reported in Fig. 4, the average crystallite size of samples TL1 and TL2 has a difference of 2 nm, but the impedance and phase angle are quite different in these samples (Fig. 6a). In this sense, the smaller crystallite size is observed for the sample TL4, but the impedance spectrum is almost the same as TL2; nevertheless, some differences are observed in the phase angle (Fig. 6b). When observing the conductivity (Fig. 6c), AC conductivity increases for all the samples after an increase in the frequency, but the increase rate in the conductivity values is observed to be the greatest for the sample with the smallest band gap (see Fig. 5 for reference), at the same time, the sample with the biggest band gap shows the smallest conductivity. Aside from the electronic nature of the materials, the conductivity and impedance are known to depend on the particle dimensions. In other words, conductivity occurs through the nanoparticles and between particles [36]. In order to elucidate what processes take place and where, an electrical circuit can be proposed for modeling the electrical behavior of the sample from the Nyquist plot (Fig. 6d). The suggested electrical model is presented in Fig. 6d, and its parameters were fitted to the experimental data. The fitting process was carried out in MATLAB, and validation of the obtained values was done through numerical

Table 2 Estimated parameters for the conductivity equation

Sample	σ_{dc}	A	n
TL1	2.65×10^{-7}	1.48×10^{-9}	0.80219
TL2	2.02×10^{-6}	3.87×10^{-10}	0.93705
TL4	3.58×10^{-6}	1×10^{-10}	1

analysis of the circuit frequency response. The results of the fitting are presented in Table 3.

The CPEp and Rp values are intended to model the electrical effects due to electrical connections to the impedance analyzer. As observed, the capacitive or reactive effects due to contact effects is almost the same for the samples TL1 and TL2. In addition, the smallest CPEp value is observed for the sample TL4; at the same time, the purely resistive effects of Rp are significantly greater for TL1 than for the other two samples. Branch 1, composed of CPE1 and R1, is related to the conductivity through the particles, and as can be observed for samples TL1 and TL2, the values of CPE1 are the same. This can be attributed to the similarity in the crystallite size; the R1 value is affected by the crystallite size. Branch 2, with the elements C2 and R2, shows the effect of conductivity between particles; as a result, the smallest C2 value is observed for the sample TL4, where the smallest crystallite size is observed. Although it has been discussed that there is a feasible effect of average crystallite size (\bar{D}), comparing the results exposed herein with others from the literature is useful. In Table 4, the conductivity analyses of TL1, TL2, and TL4 are compared to other samples with similar treatments [36, 40]. Conductivity is compared after the use of average particle size. From the data in Table 3, it can be seen that the particle size of TL1, TL2, and TL4 are within the range of sample 3 from ref [36] and sample CR from ref. [40]. As is evident, the organic extract generates a variation in the average crystallite size and also in the exhibited conductivity.

The data from Tables 2 and 4 are plotted in Fig. 7. as observed. There is an increment in the DC conductivity at the smallest crystallite size until an absolute maximum is reached at 15 nm. Then, a decrement is observed until a local minimum is achieved. Finally, after a small increment, the conductivity decreases until the absolute maximum is

Table 4 Comparison of electrochemical properties of ZnO nanoparticles reported in the literature

Sample	σ_{dc}	A	n	\bar{D}	References
1	2.57×10^{-4}	1.45×10^{-9}	0.97	66	[36]
2	9.06×10^{-5}	6.34×10^{-8}	0.71	53	
3	9.94×10^{-4}	1.16×10^{-9}	0.95	67	
MS	2.74×10^{-7}	2.54×10^{-8}	0.9	29	[40]
CR	3.93×10^{-6}	3.61×10^{-9}	1	14	

reached at 67 nm. In general terms, the DC conductivity decreases as a result of an increase of \bar{D} . Due to the effects of inter-particle contact or thorough grain boundaries, crystallites with a smaller exposed surface promote a greater conductivity among them. When the crystallite size grows, there is a greater effect of conductivity through the particles, or through the bulk of each particle, which generates an AC conductivity that is driven by the inner electrochemical properties of each particle. This is observed after the variation of n, which follows a similar behavior to σ_{dc} . However, it is observed that there is ionic conductivity for all samples. Furthermore, it can be noted that the value of A increases as a result of an increment of the average crystallite size, and also, exponential growth can be observed.

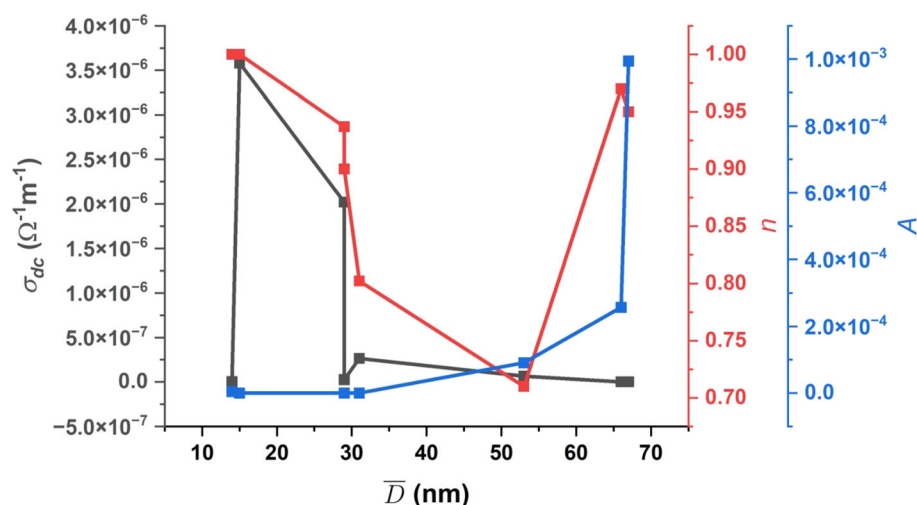
4 Conclusion

The use of environmentally friendly stabilizing agents amid biosynthesis opens up a heap of possibilities for acquiring nanomaterials with exceptional characteristics, such as the ones described in this research for TL1, TL2, and TL4. Using different amounts of *Tilia* extracts in the biosynthesis process helps to have greater control over the optical, electrochemical, and morphological properties of the obtained nanoparticles. The nanoparticle sizes rendered in this investigation are within the 33.2 to

Table 3 Estimated parameters for the equivalent electrical model

Sample	CPEp [F]	CPE1 [F]	C2 [F]	Rp [Ω]	R1 [Ω]	R2 [Ω]
TL1	10×10^{-11}	15×10^{-11}	9×10^{-11}	150×10^6	90×10^6	1×10^6
TL2	10.55×10^{-11}	15×10^{-11}	9.2×10^{-11}	10×10^6	30×10^6	2×10^6
TL4	5.9×10^{-11}	7.8×10^{-11}	2.3×10^{-11}	1.6×10^7	55.5×10^6	9×10^6

Fig. 7 Comparison of conductivity parameters of original data in this paper and data available in the literature



41.8 nm range, while the band gap values revolve around the 2.47 to 2.80 eV range. Regarding the electrochemical properties, elements C2 and R2 show the conductivity effect between particles. Thus the smallest C2 value is observed for the sample TL4 where the smallest crystallite size is observed, while for TL1 and TL2, they are similar, which is a consequence of a greater area of contact among the particles. In future work, the effect of organic reagents during synthesis on the electrochemical properties will be explored. This study proves that biosynthesis is a viable option for synthesizing nanomaterials that may have unique properties that can be implemented in abundant areas.

Acknowledgements

The authors would like to thank PRODEP for the Granted fund with number 511-6/2020-9926, and we gratefully acknowledge the use of TEM facilities at the TEM Laboratory of Universidad de Sonora.

Author contributions

HEG-G: conceptualization, methodology, writing-review and editing. LC-A: investigation, data curation and visualization. RML-G: methodology, formal analysis, and writing original draft. MEM-R: formal-analysis and writing review and editing. FNM-R: formal analysis, visualization, and software. And PAL: conceptualization, resources, supervision, and validation.

Funding

The authors have not disclosed any funding.

Data availability

All data generated in this study are included in this article.

Declarations

Conflict of interest There are no conflicts to declare.

References

1. M. Shkir, K.V. Chandekar, B.M. Alshehri, A. Khan, S. AlFaify, M.S. Hamdy, A remarkable enhancement in photocatalytic activity of facilely synthesized Terbium@Zinc oxide nanoparticles by flash combustion route for optoelectronic applications. *Appl. Nanosci.* **10**, 1811–1823 (2020). <https://doi.org/10.1007/s13204-019-01236-6>
2. H. Çolak, E. Karaköse, F. Duman, High optoelectronic and antimicrobial performances of green synthesized ZnO nanoparticles using *Aesculus hippocastanum*. *Environ. Chem. Lett.* **15**, 547–552 (2017). <https://doi.org/10.1007/s10311-017-0629-z>
3. N. Matinise, X.G. Fuku, K. Kaviyarasu, N. Mayedwa, M. Maaza, ZnO nanoparticles via *Moringa oleifera* green synthesis: physical properties & mechanism of formation. *Appl. Surf. Sci.* **406**, 339–347 (2017). <https://doi.org/10.1016/j.apsusc.2017.01.219>
4. V.N. Kalpana, V. Devi Rajeswari, A review on green synthesis, biomedical applications, and toxicity studies of ZnO

- NPs. *Bioinorg. Chem. Appl.* **2018**, 3569758 (2018). <https://doi.org/10.1155/2018/3569758>
5. A. Miri, N. Mahdinejad, O. Ebrahimi, M. Khatami, M. Sarani, Zinc oxide nanoparticles: biosynthesis, characterization, antifungal and cytotoxic activity. *Mater. Sci. Eng. C* **104**, 109981 (2019). <https://doi.org/10.1016/j.msec.2019.109981>
 6. C.G. Yuan, C. Huo, S. Yu, B. Gui, Biosynthesis of gold nanoparticles using *Capsicum annuum* var. Grossum pulp extract and its catalytic activity. *Phys. E Low Dimens. Syst. Nanostruct.* **85**, 19–26 (2017). <https://doi.org/10.1016/j.phys.e.2016.08.010>
 7. K. Velsankar, S. Sudhahar, G. Maheshwaran, M. Krishna Kumar, Effect of biosynthesis of ZnO nanoparticles via cucurbita seed extract on *Culex tritaeniorhynchus* mosquito larvae with its biological applications. *J. Photochem. Photobiol. B Biol.* **200**, 111650 (2019). <https://doi.org/10.1016/j.jphotobiol.2019.111650>
 8. S. Sheik Mydeen, R. Raj Kumar, M. Kottaisamy, V.S. Vasantha, Biosynthesis of ZnO nanoparticles through extract from *Prosopis juliflora* plant leaf: antibacterial activities and a new approach by rust-induced photocatalysis. *J. Saudi Chem. Soc.* **24**, 393–406 (2020). <https://doi.org/10.1016/j.jscs.2020.03.003>
 9. M.S. Khan, P.P. Dhavan, D. Ratna, N.G. Shimpi, Ultrasonic-assisted biosynthesis of ZnO nanoparticles using *Sonneratia alba* leaf extract and investigation of its photocatalytic and biological activities. *J. Clust. Sci.* (2021). <https://doi.org/10.1007/s10876-021-02036-1>
 10. R. Hassanien, D.Z. Husein, M.F. Al-Hakkani, Biosynthesis of copper nanoparticles using aqueous *Tilia* extract: antimicrobial and anticancer activities. *Heliyon* **4**, e01077 (2018). <https://doi.org/10.1016/j.heliyon.2018.e01077>
 11. Z. Konvičková, V. Holišová, M. Kolenčík, T. Niide, G. Kratošová, M. Umetsu, J. Seidlerová, Phytosynthesis of colloidal Ag-AgCl nanoparticles mediated by *Tilia* sp. leachate, evaluation of their behaviour in liquid phase and catalytic properties. *Colloid Polym. Sci.* **296**, 677–687 (2018). <https://doi.org/10.1007/s00396-018-4290-2>
 12. K.O. Saygi, E. Cacan, Antioxidant and cytotoxic activities of silver nanoparticles synthesized using *Tilia cordata* flowers extract. *Mater. Today Commun.* **27**, 102316 (2021). <https://doi.org/10.1016/j.mtcomm.2021.102316>
 13. W.J. Aziz, M.A. Abid, E.H. Hussein, Biosynthesis of CuO nanoparticles and synergistic antibacterial activity using mint leaf extract. *Mater. Technol.* **35**, 447–451 (2020). <https://doi.org/10.1080/10667857.2019.1692163>
 14. V. Holišová, M. Urban, Z. Konvičková, M. Kolenčík, P. Mančík, J. Slobotinský, G. Kratošová, D. Plachá, Colloidal stability of phytosynthesised gold nanoparticles and their catalytic effects for nerve agent degradation. *Sci. Rep.* **11**, 4071 (2021). <https://doi.org/10.1038/s41598-021-83460-1>
 15. A. Corciova, B. Ivanescu, C. Tuchilus, A. Fifere, F. Doroftei, A.L. Lungoci, N. Marangoci, C. Mircea, Biosynthesis of silver nanoparticles (agnps) using *tilia cordata* flowers extracts and evaluation of some biological activities. *Environ. Eng. Manag. J.* **17**, 2957–2968 (2018)
 16. G. Nagaraju, G.C. Shivaraju, G. Banuprakash, D. Rangappa, Photocatalytic activity of ZnO nanoparticles: synthesis via solution combustion method. *Mater. Today Proc.* **4**, 11700–11705 (2017). <https://doi.org/10.1016/j.matpr.2017.09.085>
 17. G. Sharmila, M. Thirumarimurugan, C. Muthukumaran, Green synthesis of ZnO nanoparticles using *Tecoma castanifolia* leaf extract: characterization and evaluation of its antioxidant, bactericidal and anticancer activities. *Microchem. J.* **145**, 578–587 (2019). <https://doi.org/10.1016/j.microc.2018.11.022>
 18. A. Siger, W. Antkowiak, K. Dwiecki, E. Rokosik, M. Rudzińska, Nutlets of *Tilia cordata* Mill. and *Tilia platyphyllos* Scop. source of bioactive compounds. *Food Chem.* **346**, 128888 (2021). <https://doi.org/10.1016/j.foodchem.2020.128888>
 19. K. Velsankar, S. Sudhahar, G. Parvathy, R. Kalliammal, Effect of cytotoxicity and antibacterial activity of biosynthesis of ZnO hexagonal shaped nanoparticles by *Echinochloa frumentacea* grains extract as a reducing agent. *Mater. Chem. Phys.* **239**, 121976 (2020). <https://doi.org/10.1016/j.matchemphys.2019.121976>
 20. D.V. Pandi, V. Saraswathi, N. Muthukumarasamy, S. Agilan, P. Balraju, D. Velauthapillai, C-axis oriented ZnO nanorods based quantum dot solar cells. *Opt. Mater. (Amst)* **112**, 110774 (2021). <https://doi.org/10.1016/j.optmat.2020.110774>
 21. D. Bharathi, R.H. Krishna, V. Singh, N. Kottam, B. Siddlingeshwar, One pot synthesis of C-dots and study on its interaction with nano ZnO through fluorescence quenching. *J. Lumin.* **190**, 328–334 (2017). <https://doi.org/10.1016/j.jlum.2017.05.077>
 22. S. Rajeshkumar, S.V. Kumar, A. Ramaiah, H. Agarwal, T. Lakshmi, S.M. Roopan, Biosynthesis of zinc oxide nanoparticles using *Mangifera indica* leaves and evaluation of their antioxidant and cytotoxic properties in lung cancer (A549) cells. *Enzyme Microb. Technol.* **117**, 91–95 (2018). <https://doi.org/10.1016/j.enzmictec.2018.06.009>
 23. E. Nagaraj, P. Shanmugam, K. Karuppannan, T. Chinnasamy, S. Venugopal, The biosynthesis of a graphene oxide-based zinc oxide nanocomposite using *Dalbergia latifolia* leaf extract and its biological applications. *New. J. Chem.* **44**, 2166–2179 (2020). <https://doi.org/10.1039/C9NJ04961D>
 24. S. Vijayakumar, C. Krishnakumar, P. Arulmozhi, S. Mahadevan, N. Parameswari, Biosynthesis, characterization and antimicrobial activities of zinc oxide nanoparticles from

- leaf extract of *Glycosmis pentaphylla* (Retz.) DC. Microb. Pathog. **116**, 44–48 (2018). <https://doi.org/10.1016/j.micpath.2018.01.003>
25. E. Vidhya, S. Vijayakumar, S. Prathipkumar, P.K. Praseetha, Green way biosynthesis: characterization, antimicrobial and anticancer activity of ZnO nanoparticles. Gene Rep. **20**, 100688 (2020). <https://doi.org/10.1016/j.genrep.2020.100688>
26. S. Vijayakumar, S. Mahadevan, P. Arulmozhi, S. Sriram, P.K. Praseetha, Green synthesis of zinc oxide nanoparticles using *Atalantia monophylla* leaf extracts: characterization and antimicrobial analysis. Mater. Sci. Semicond. Process. **82**, 39–45 (2018). <https://doi.org/10.1016/j.mssp.2018.03.017>
27. S. Vijayakumar, M. Nilavukkarasi, B. Sakthivel, Bio-synthesized zinc oxide nanoparticles for anti-tuberculosis agent: scientifically unexplored. Gene Rep. **20**, 100764 (2020). <https://doi.org/10.1016/j.genrep.2020.100764>
28. Y. Hou, Y. Hou, Y. Ren, Y. Shi, X. Jin, Y. Dong, H. Zhang, C. aromaticus leaf extract mediated synthesis of zinc oxide nanoparticles and their antimicrobial activity towards clinically multidrug-resistant bacteria isolated from pneumonia patients in nursing care. Mater. Res. Express **7**, 95015 (2020). <https://doi.org/10.1088/2053-1591/abb427>
29. T. Varadavenkatesan, E. Lyubchik, S. Pai, A. Pugazhendhi, R. Vinayagam, R. Selvaraj, Photocatalytic degradation of rhodamine B by zinc oxide nanoparticles synthesized using the leaf extract of *Cyanometra ramiflora*. J. Photochem. Photobiol. B Biol. **199**, 111621 (2019). <https://doi.org/10.1016/j.jphoto.2019.111621>
30. M. Zare, K. Namratha, K. Byrappa, D.M. Surendra, S. Yalappa, B. Hungund, Surfactant assisted solvothermal synthesis of ZnO nanoparticles and study of their antimicrobial and antioxidant properties. J. Mater. Sci. Technol. **34**, 1035–1043 (2018). <https://doi.org/10.1016/j.jmst.2017.09.014>
31. M. Ahmad, W. Rehman, M.M. Khan, M.T. Qureshi, A. Gul, S. Haq, R. Ullah, A. Rab, F. Mena, Phytogenic fabrication of ZnO and gold decorated ZnO nanoparticles for photocatalytic degradation of rhodamine B. J. Environ. Chem. Eng. **9**, 104725 (2021). <https://doi.org/10.1016/j.jece.2020.104725>
32. L. Chen, I. Batjikh, J. Hurh, Y. Han, Y. Huo, H. Ali, J.F. Li, E.J. Rupa, J.C. Ahn, R. Mathiyalagan, D.C. Yang, Green synthesis of zinc oxide nanoparticles from root extract of *Scutellaria baicalensis* and its photocatalytic degradation activity using methylene blue. Optik **184**, 324–329 (2019). <https://doi.org/10.1016/j.ijleo.2019.03.051>
33. J.B. Coulter, D.P. Birnie, Assessing Tauc plot slope quantification: ZnO thin films as a model system. Phys. Status Solidi **255**, 1700393 (2018). <https://doi.org/10.1002/pssb.201700393>
34. M.N.H. Mia, M.F. Pervez, M.K. Hossain, M. Reefaz Rahman, M.J. Uddin, M.A. Al Mashud, H.K. Ghosh, M. Hoq, Influence of mg content on tailoring optical bandgap of Mg-doped ZnO thin film prepared by sol-gel method. Results Phys. **7**, 2683–2691 (2017). <https://doi.org/10.1016/j.rinp.2017.07.047>
35. A. Taşdemir, R. Aydın, A. Akkaya, N. Akman, Y. Altınay, H. Çetin, B. Şahin, A. Uzun, E. Ayyıldız, A green approach for the preparation of nanostructured zinc oxide: characterization and promising antibacterial behaviour. Ceram. Int. **47**, 19362–19373 (2021). <https://doi.org/10.1016/j.ceramint.2021.03.273>
36. M.E. Martínez-Rosas, H.E. Garrafa-Gálvez, O. Nava, F.N. Murrieta-Rico, M.J. Chinchillas-Chinchillas, A. Carrillo-Castillo, P.A. Luque, Electrochemical impedance characterization of ZnO semiconductor nanoparticles biosynthesized with *Verbascum thapsus*. J. Mater. Sci. Mater. Electron. **32**, 10510–10519 (2021). <https://doi.org/10.1007/s10854-021-05706-y>
37. A. Dhahri, E. Dhahri, E.K. Hlil, Electrical conductivity and dielectric behaviour of nanocrystalline La_{0.6}Gd_{0.1}Sr_{0.3}Mn_{0.75}Si_{0.25}O₃. RSC Adv. **8**, 9103–9111 (2018). <https://doi.org/10.1039/C8RA00037A>
38. M. Chaari, A. Matoussi, Structural and dielectric properties of undoped ZnO pellets prepared by solid state route. Appl. Phys. A **116**, 1149–1160 (2014). <https://doi.org/10.1007/s00339-013-8199-9>
39. O. Nava, F.N. Murrieta-Rico, M.E. Martínez-Rosas, M.J. Chinchillas-Chinchillas, H.E. Garrafa-Gálvez, A.R. Vilchis-Nestor, P.A. Luque, Evaluation of electrochemical properties of zinc oxide based semiconductor nanoparticles biosynthesized with *Mentha spicata* for optoelectronic applications. Mater. Lett. **275**, 128101 (2020). <https://doi.org/10.1016/j.matlet.2020.128101>
40. F.N. Murrieta-Rico, M. Luque, G. Romo-Cárdenas, P.A. Luque, Evaluation of naturally synthesized ZnO for sensing applications using EIS. Mater. Today: Proc. **47**, 1676–1681 (2021). <https://doi.org/10.1016/j.matpr.2021.05.465>

Publisher's Note Springer Nature remains neutral with regard to jurisdictional claims in published maps and institutional affiliations.

Springer Nature or its licensor (e.g. a society or other partner) holds exclusive rights to this article under a publishing agreement with the author(s) or other rightsholder(s); author self-archiving of the accepted manuscript version of this article is solely governed by the terms of such publishing agreement and applicable law.